

## First-Order Isostructural Mott Transition in Highly Compressed MnO

C. S. Yoo, B. Maddox, J.-H. P. Klepeis, V. Iota, W. Evans, and A. McMahan

*Lawrence Livermore National Laboratory, Livermore, California 94551, USA*

M. Y. Hu, P. Chow, M. Somayazulu, and D. Häusermann

*HP-CAT, Advanced Photon Source, Argonne National Laboratory, Argonne, Illinois 60439, USA*

R. T. Scalettar and W. E. Pickett

*University of California, Davis, California 95616, USA*

(Received 14 June 2004; published 22 March 2005)

We present evidence for an isostructural, first-order Mott transition in MnO at  $105 \pm 5$  GPa, based on high-resolution x-ray emission spectroscopy and angle-resolved x-ray diffraction data. The pressure-induced structural and spectral changes provide a coherent picture of MnO phase transitions from paramagnetic *B1* to antiferromagnetic distorted *B1* at 30 GPa, to paramagnetic *B8* at 90 GPa, and to diamagnetic *B8* at  $105 \pm 5$  GPa. The last is the Mott transition, accompanied by a significant loss of magnetic moment, a  $\sim 6.6\%$  volume collapse and the insulator-metal transition as demonstrated by recent resistance measurements.

DOI: 10.1103/PhysRevLett.94.115502

PACS numbers: 62.50.+p, 61.10.-i, 64.30.+t, 64.70.Kb

Mott's seminal work on how insulating character may arise out of the electron-electron repulsion used a 3*d* transition metal monoxide, NiO, as an example and suggested its pressure-induced metallization, the Mott transition [1]. Yet for 55 years the Mott transition in these archetypal Mott insulators MnO, FeO, CoO, and NiO has eluded detection at room temperature due to the high pressures required. Recent resistivity measurements using "designer" diamond anvils, however, have seen this insulator-metal transition in MnO, a 5-order of magnitude decrease in resistance between 90 and 106 GPa [2]. In this Letter, we present x-ray emission spectroscopy and x-ray diffraction data which not only suggest that the Mott transition in MnO is a far richer phenomenon than just the onset of metallization, but that it also exhibits profound similarities to transitions in the lanthanides and actinides as has been predicted [3] and thus furthers our general understanding of electron-correlation driven phase transitions.

Our results are summarized in the conceptual phase diagram for MnO presented in Fig. 1, where phases are labeled by structure (*B1* for rocksalt, *dB1* for a rhombohedral distortion of *B1*, and *B8* for NiAs) and magnetic order (PM, AFM, and DM for paramagnetic, antiferromagnetic, and diamagnetic, respectively). Figure 1 is topologically equivalent to the combined structural [4] and magnetic [5] phase diagrams proposed for FeO, and is quantified for MnO by the ambient-pressure 118 K Néel temperature [6] (diamond), shock data [7] (star), the observed 300 K metallization [2], and our three room-temperature transitions (open circles). Here we concur with earlier 300 K work on MnO in the 30–90 GPa stability field for the *dB1* phase as well as a dense *B8* phase above 120 GPa exhibiting metallic luster [8]. However, the earlier work indicated an unknown "intermediate" phase between 90 and 120 GPa

which we have now resolved. We identify the Mott transition at 300 K as the  $105 \pm 5$  GPa point at which we find simultaneously a transition from a PM to a DM state defined by a significant loss of the Hund's rules 3*d*<sup>5</sup> magnetic moments, a first-order isostructural transition in the *B8* phase with a  $\sim 6.6\%$  volume change, and the insulator-metal transition [2]. It has been argued previously [5,9] for compressed FeO that AFM order is lost first (corresponding to the 90 GPa transition in MnO) and then at a higher pressure one should have a PM to DM transition (the 105 GPa point in MnO). The latter PM–DM transition has not yet been seen in FeO nor the 300 K metallization

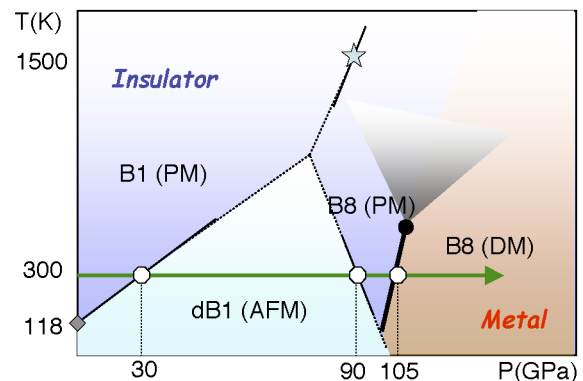


FIG. 1 (color online). The conceptual phase diagram of MnO based on the present static high-pressure data (open circles), the previous shock data (star) [7], and the ambient-pressure Néel temperature (diamond) [6]. The thick phase line signifies the first-order isostructural Mott transition which simultaneously accompanies with loss of magnetic moment, a large volume collapse and metallization, and should end at the critical point (solid circle). The gray fan above the critical point represents a smooth crossover to metallic behavior at high temperature.

[4], perhaps for kinetic reasons, although FeO has been metallized for temperatures greater than 1000 K at pressures above 70 GPa [10]. Local density functional calculations have predicted a region of high-pressure  $B8$  stability [11] for MnO as well as a magnetic collapse [12] at 149 GPa.

High purity MnO powder samples (99 + %, Alfa-Aesar) were loaded in diamond anvil cells together with mineral oil. Mineral oil provides a reasonably quasihydrostatic condition, important for probing subtle structural/spectral changes in MnO at high pressures. The ruby spectrum of the sample remains relatively sharp with well resolved  $R_1$  and  $R_2$  lines at least to 100 GPa above which the lines get rapidly broadened. The pressure was determined at the same spot before and after each x-ray spectral measurement, showing a relatively small pressure difference well within 2 GPa at all pressures. The pressure gradient was estimated to be about 3 GPa across the 20  $\mu\text{m}$  sample at 100 GPa. We used beveled diamond anvils (100  $\mu\text{m}$  flat over 300  $\mu\text{m}$  culet) with a relatively small sample chamber ( $\sim 50 \mu\text{m}$  hole) in a  $\sim 30 \mu\text{m}$  thick gasket made of either Re for x-ray diffraction or x-ray translucent Be for x-ray emission spectroscopy.

We have used x-ray emission spectroscopy (XES) to probe the  $3d$  magnetic moments in highly compressed MnO. These experiments were carried out using intense monochromatic x rays (10.225 KeV) from an undulator at the 161DD at the Advanced Photon Source (APS). The incident x ray was focused to  $\sim 20 \times 50 \mu\text{m}$  at the sample by using a pair of 1 m long K-B focusing mirrors. X-ray fluorescence was then collected at  $90^\circ$  from the incident x ray to reduce the elastically scattered background, by using a 1 m Rowland circle spectrometer arranged on a vertical plane. A spherically bent Si(333) single crystal analyzer (100 mm in diameter) was used to refocus the fluorescence onto a Si detector (Amp Tek). The Bragg angle is  $66.06^\circ$  at the  $K\beta$  emission energy 6.490 KeV. The energy calibration has been done using Mn foil. This configuration provides approximately 0.5 eV energy resolution.

The resultant  $K\beta$  emission lines for compressed MnO shown in Fig. 2 represent transitions associated with the  $1s$  core-hole decays to the  $3p$  states in Mn, which consist of two branches,  $K\beta_{1,3}$  ( ${}^7P$  states) and  $K\beta'$  ( ${}^5P$  states), split by about 16 eV as a result of the  $3p$  core-hole  $3d$  electron exchange interaction [13]. Therefore, the energy separation and the intensity ratio of the two bands are proportional to the magnitude of electron exchange interaction and the net spin of  $3d$  bands, respectively. Most significantly, the intensity of the  $K\beta'$  band is sensitive to the local magnetic moment, as has been well established in many  $3d$  transition metals and transition metal compounds [14].

The XES results in Fig. 2 show the pressure-induced changes of the  $K\beta$  spectra to 132 GPa. These spectra are overlaid in three groups depending on pressure: the first

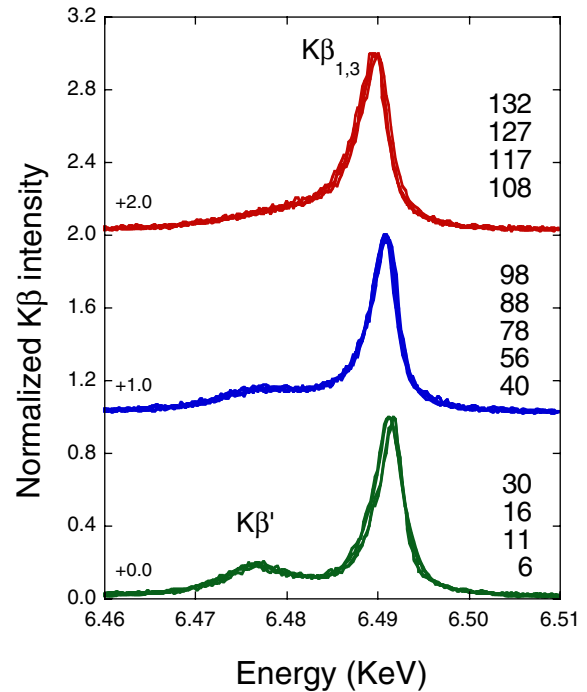


FIG. 2 (color online).  $K\beta$  x-ray emission branches of MnO at high pressures (all in GPa), showing subtle spectral changes in the  $K\beta_{1,3}$  peak positions and the  $K\beta'$  intensities above 30 and 98 GPa (also shown in Fig. 3). The apparent absence of a  $K\beta'$  peak above 108 GPa signifies the loss of the magnetic moment.

below 30 GPa with distinctive  $K\beta'$  intensity, the second between 40 and 98 GPa where the  $K\beta'$  intensity is noticeably reduced yet apparent, and the third above 108 GPa where it is no longer possible to identify a  $K\beta'$  peak, indicating a significant loss of magnetic moment in this material. It is also apparent that the peak position of the

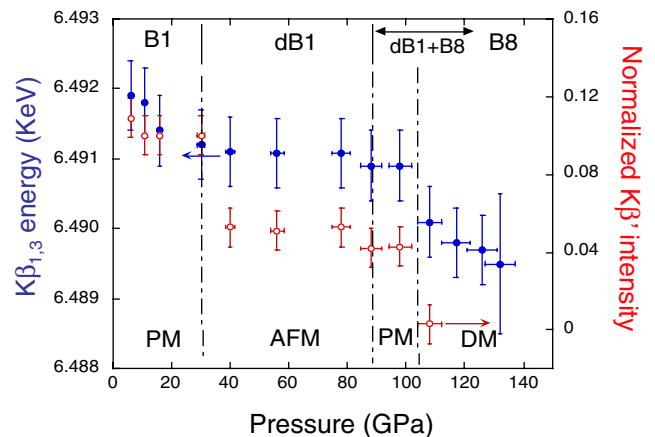


FIG. 3 (color online). The pressure-induced spectral changes of MnO, illustrating three first-order electronic phase transitions at 30, 90, and 103 GPa. The first two correspond to the  $B1$  (PM) to  $dB1$  (AFM) and the  $dB1$  (AFM) to  $B8$  (PM) transitions, respectively, whereas the third occurs within the  $B8$  structure following the  $dB1$  to  $B8$  transition at 90 GPa.

$K\beta_{1,3}$  band is shifted toward lower energy by about 1 eV as the pressure increases from one to the other group. A similar shift of the  $K\beta_{1,3}$  peak was also observed in FeO, but was unexplained [5].

Figure 3 plots the pressure dependence of both the  $K\beta_{1,3}$  peak position and a normalized  $K\beta'$  peak intensity obtained by subtracting the 132 GPa spectrum from each spectra obtained below this pressure. There are three evident discontinuous changes in one or both diagnostics, first near 30 GPa at the onset of the  $B1$  (PM) to  $dB1$  (AFM) phase transition, then near 90 GPa, and finally the vanishing  $K\beta'$  peak at 103 GPa signifying the loss of the moment. We suggest that the second 90 GPa signature in MnO corresponds to the AFM to PM transition described for FeO [5]. Hubbard model calculations [15] show that the local moment is reduced with increasing antiferromagnetic correlations (decreasing temperature) at strong coupling, yet behaves the opposite way for weak coupling. Presuming that these correlations change discontinuously across the AFM phase lines, one would expect the moment for compressed MnO to drop both on entering the AFM region at 30 GPa (strong coupling) and yet again leaving it at 90 GPa (weaker coupling) as is indeed observed in the  $K\beta'$  signature in Fig. 3. The third electronic phase transition near 103 GPa occurs above 90 GPa where the  $dB1$  phase transforms to the intermediate phase in Ref. [8], but below 120 GPa where the intermediate phase transforms to the  $B8$  phase. As discussed below, this apparent discrepancy is due to the ill characterized intermediate phase.

In order to resolve these structural issues, angle-dispersive x-ray diffraction experiments were carried out using microfocused ( $\sim 10 \mu\text{m}$ ) monochromatic ( $0.3678 \text{ \AA}$ ) x rays at the 161DB at the APS. The x-ray diffraction patterns were recorded on an online image plate, and the Debye-Scherrer diffraction image was then analyzed by using the FIT2D and GSAS programs. The results are summarized in Figs. 4 and 5, and they indicate MnO transforms from the  $B1$  to the  $dB1$  phase at 30 GPa, to the intermediate phase at 90 GPa, and to  $B8$  at around 120–130 GPa, similarly to the previous report [8]. However, the present data further reveal that the intermediate phase can be interpreted in terms of a mixture between the  $dB1$  and  $B8$  phases. All diffraction lines at 90 GPa in Fig. 4 are accounted for by either  $dB1$  and  $B8$  indexing with an exception near the broad 102 reflection of  $dB1$ . This broad feature, on the other hand, can be easily understood in terms of a superlattice reflection ( $1/2, 1/2, 5/2$ ) near the 102 reflection arising from lattice distortion across the displacive  $dB1$  to  $B8$  phase transition. The refined intensities are well matched to the measured ones for all three phases.

There is a precedent for such mixed phase behavior in displacive transitions. Note first that there is only a small difference between  $dB1$  and  $B8$  structures: the  $dB1$  is a six-layer structure  $A(O)c'(Mn)B(O)a'(Mn)C(O)b'(Mn)$ ,

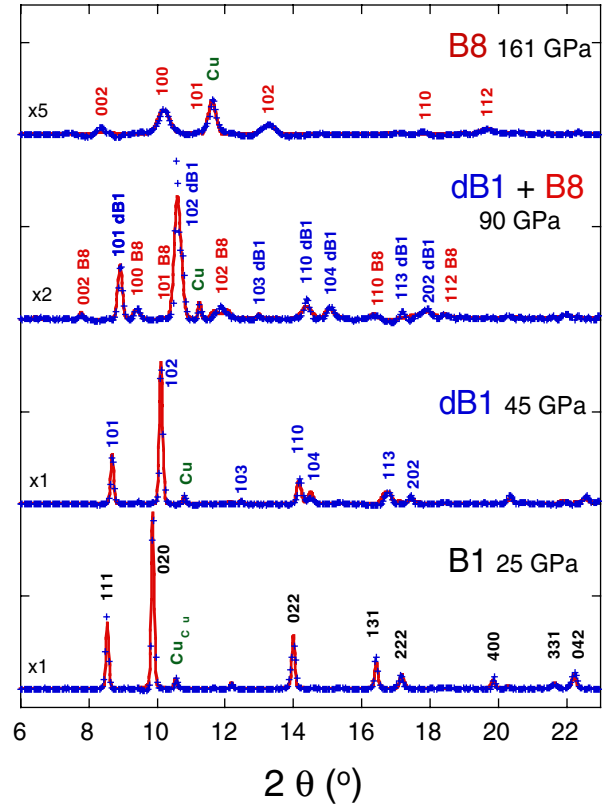


FIG. 4 (color online). The measured (blue crosses) and refined (red lines) x-ray diffraction patterns of MnO phases. Miller indices are marked for each phase, together with the 111 reflection of Cu used as an internal pressure marker.

whereas the  $B8$  is a four-layer  $a(\text{Mn})B(\text{O})a(\text{Mn})C(\text{O})$ . Therefore, the  $dB1$  to  $B8$  transition requires a slight displacement of oxygen atoms from distorted octahedral sites with three quasinearest Mn-O distances, 1.70, 2.17, and 2.24  $\text{\AA}$  to perfect trigonal prism sites with all equal Mn-O distance, 2.04  $\text{\AA}$ . Such a displacive transition between two energetically similar structures often results in relatively large hysteresis in pressure and thus in two phases which coexist over an extended pressure range. The examples of similar displacive transitions resulting in commensurate mixtures and superlattice structures are numerous, particularly of electronically driven phase transitions including similar Mott transitions in other materials,  $\text{Fe}_2\text{O}_3$  [16] and  $\text{FeI}_2$  [17], and the previous theoretical interpretation of FeO [18].

Figure 5 shows the present results for specific volume and  $c/a$  ratio (inset) versus pressure. Note that indexing as in the 90 GPa panel of Fig. 4 provides values of these quantities for *both*  $dB1$  and  $B8$  phases throughout the intermediate pressure region between 90 and 120 GPa. Moreover, the fact that the  $dB1$  specific volume and  $c/a$  ratio decrease seamlessly without apparent discontinuity across the transition at 90 GPa is a stringent test and validation of our analysis. Note that the  $B8$  phase has

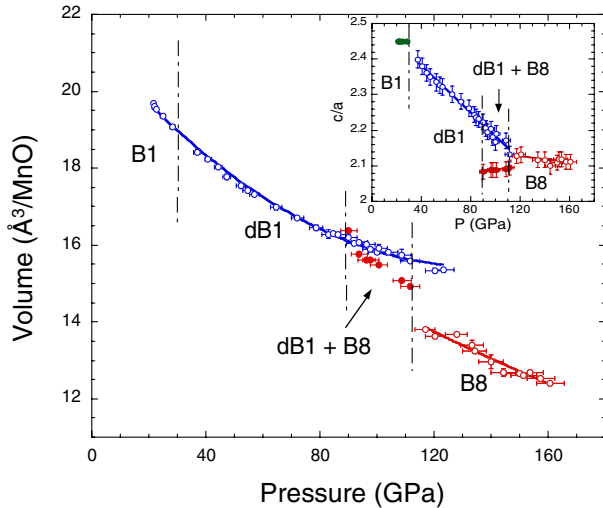


FIG. 5 (color online). The specific volume and the  $c/a$  ratio (inset) of MnO phases as a function of pressure. Note the discontinuous changes of the specific volume and the  $c/a$  ratio at 110 GPa, indicating that MnO undergoes an isostructural phase transition with 6.6% volume collapse. This transition coincides within experimental uncertainties with the moment loss (see Fig. 3) and the insulator-metal transition in Ref. [2].

nearly the same specific volume as the  $dB1$  to 90 GPa, but becomes about 4.5% denser by 110 GPa. Furthermore, the compression curve of the  $B8$  phase exhibits a discontinuous volume change of  $\sim 6.6\%$  at around 110 GPa, that is, a first-order isostructural transition within the  $B8$  phase. A similar discontinuous change is also apparent in the  $c/a$  ratio of the  $B8$  structure (Fig. 5, inset), further supporting the first-order isostructural phase transition.

The present spectral and diffraction data together with the recent resistance data [2] provide a coherent picture of the Mott transition in MnO. Recall that MnO loses its  $K\beta'$  intensity completely above  $103 \pm 5$  GPa, indicating loss of moment, has an isostructural volume collapse of 6.6% at  $\sim 110$  GPa, and the resistance data [2] exhibit a sharp (nearly 3 orders of magnitude drop) from  $10^1 \Omega$  at 103 GPa to  $10^2 \Omega$  at 105 GPa consistent with our visual observation of metallic luster above about 108 GPa. These pressures are all close enough to be interpreted as manifestations of the same pressure-induced Mott transition in MnO: (i) significant loss of magnetic moment, (ii) large isostructural volume collapse, and (iii) the insulator-metal transition. Although similarities between the electron-correlation driven transitions in the  $3d$  monoxides and the  $4f$ - and  $5f$ -electron metals were predicted years ago [3], it is truly striking that these three signatures observed here for the archetypal Mott transition in MnO are *all* observed at the volume-collapse transitions in the lantha-

nide and actinide metals, taking “metallization” to refer more generally to the behavior of the respective  $d$  or  $f$  spectral weight near the Fermi level, and acknowledging that the volume collapse need not always be isostructural [19,20]. There may well be important differences such as whether in the low temperature limit the  $d$  or the  $f$  spectral weight at the Fermi level abruptly or continuously disappears on the “insulator” side of the transition. Nevertheless, the similarities are also profound and should be incorporated in any general theory of electron-correlation driven transitions.

We thank Dr. Chi-Chang Kao for lending us his Si analyzer. This work has been supported by the LDRD-04-ERD-020 and PDRP programs at the LLNL, University of California, under the auspices of the U.S. DOE under Contract No. W-7405-ENG-48 and by the Stockpile Stewardship Academic Alliances Program under DOE Grant No. DE-FG03-03NA00071. Use of the HPCAT facility was supported by DOE-BES, DOE-NNSA (CDAC), NSF, DoD-TACOM, and the W.M. Keck Foundation.

- [1] M.F. Mott, Proc. Phys. Soc. London, Sect. A **62**, 416 (1949); *Metal Insulator Transitions* (Taylor and Francis, London, 1990).
- [2] J.R. Patterson *et al.*, Phys. Rev. B **69**, 220101 (2004).
- [3] B. Johansson, Phys. Rev. B **15**, 5890 (1977).
- [4] H.K. Mao *et al.*, Earth Planet. Inter. **96**, 135 (1996).
- [5] J. Badro *et al.*, Phys. Rev. Lett. **83**, 4101 (1999).
- [6] D. Bloch, C. Vettier, and P. Burel, Phys. Lett. A **75**, 301 (1980).
- [7] Y. Syono, RIKEN Rev. **27**, 72 (2000).
- [8] T. Kondo *et al.*, J. Appl. Phys. **87**, 4153 (2000).
- [9] M.P. Pasternak *et al.*, Phys. Rev. Lett. **79**, 5046 (1997).
- [10] E. Knittle and R. Jeanloz, Geophys. Res. Lett. **13**, 1541 (1986).
- [11] Z. Fang *et al.*, Phys. Rev. Lett. **81**, 1027 (1998); Phys. Rev. B **59**, 762 (1999).
- [12] R.E. Cohen, I.I. Mazin, D.G. Isaak, Science **275**, 654 (1997).
- [13] F. deGroot, Chem. Rev. **101**, 1779 (2001).
- [14] G. Peng *et al.*, J. Am. Chem. Soc. **116**, 2914 (1994).
- [15] T. Paiva *et al.*, Phys. Rev. B **63**, 125116 (2001).
- [16] M.P. Pasternak *et al.*, Phys. Rev. Lett. **82**, 4663 (1999).
- [17] G. Kh. Rozenberg *et al.*, Phys. Rev. B **68**, 64105 (2003).
- [18] I.I. Mazin, Y. Fei, R. Downs, and R. Cohen, Am. Mineral. **83**, 451 (1998).
- [19] A.K. McMahan, C. Huscroft, R.T. Scalettar, and E.L. Pollock, J. Comput.-Aided Mater. Des. **5**, 131 (1998).
- [20] U. Benedict, W.A. Grosshans, and W.B. Holzapfel, Physica (Amsterdam) **144B**, 14 (1986).